

The auto-correlation function of the extragalactic background light: I. Measuring gravitational shear

L. Van Waerbeke¹, Y. Mellier^{1,2,3}, P. Schneider², B. Fort³, and G. Mathez¹

¹ LAT, URA285. Observatoire Midi-Pyrénées 14, avenue Edouard Belin 31400 Toulouse, France

² Max-Planck-Institut für Astrophysik, Karl-Schwarzschild-Str. 1 Postfach 1523, 85740 Garching, Germany

³ DEMIRM, Observatoire de Paris, 61 Avenue de l'Observatoire 75014 Paris, France

⁴ Institut d'Astrophysique de Paris, 98 bis boulevard Arago 75014 Paris, France

Received pretty soon, I bet ; Accepted immediately

Abstract. A new method for measuring the shear induced by gravitational light deflection is proposed. It is based on analyzing the anisotropy induced in the auto-correlation function of the extragalactic background light which is produced by very faint distant galaxies. The auto-correlation function can be measured 'locally', and its anisotropy is caused by the tidal gravitational field of the deflecting mass distribution in the foreground of these faint background galaxies.

Since the method does not require individual galaxy detection, it can be used to measure the shear of extremely faint galaxies which are not detectable individually, but are present in the noise. The shear estimated from the auto-correlation function of the noise provides an independent measurement which can be compared to the shear obtained from the distortion of individual galaxy images. Combining these two independent estimates clearly increases the sensitivity of shear measurements. In addition, our new method may allow to determine the local magnification caused by the deflector if the auto-correlation function is caused by a large number density of faint galaxies; in this case, the intrinsic auto-correlation function may provide a 'standard source' with respect to which shear and magnification can be obtained. Applications to real and synthetic data are shown and the feasibility of our new method is demonstrated. In particular, we present the shear maps obtained with our new method for the double QSO 2345+007 and the cluster Cl0024+16 and compare them to published shear maps.

by gravitational shear maps almost directly the total mass projected near the line of sight to these faint galaxies regardless of its dynamical state. Recent theoretical and observational work on galaxy-galaxy lensing (Brainerd et al., 1996, Schneider & Rix 1996), weak lensing in rich lensing-clusters (Kaiser & Squires 1993, Seitz & Schneider 1995, Bonnet et al. 1994, hereafter BMF; Fahlmann et al. 1994, Squires et al. 1996, Seitz et al. 1996), and from large scale structures (Blandford et al. 1991, Kaiser 1992, Villumsen 1996) justifies the expectation that outstanding results on the mass distributions of these systems will be available in a near future which will solve numerous puzzling issues on the (dark) mass distribution, on the number density of dark halos, and on the relation between light and mass of gravitational structures.

In the work quoted above, the shear is inferred from the ellipticity measured on individual background galaxies (we shall refer to this method in the following as 'standard method', to contrast it to our new method). In the case of weak lensing, the induced distortion is extremely small which makes the measurement of the ellipticity from ground-based telescopes images a major concern. The measurement and the various instrumental and atmospheric corrections of shape parameters have been discussed by Kaiser, Squires & Broadhurst (1995) and Bonnet & Mellier (1995, hereafter, BM). From these investigations, one finds that dramatic limitations come from rather poor signal-to-noise ratios of images at very weak shear level. Ultra-deep CCD images on wide fields allow the computation of the averaged ellipticity on a large area with many galaxies which increases notably the signal-to-noise ratio. However, this strategy has important shortcomings:

1. The CCD area over which ellipticities can be averaged to obtain a local estimate of the shear is limited to a typical scale across which the magnification matrix is approximately constant. Hence, it depends on the typical angular scale of the gravitational structure. Furthermore, averaging on large areas decreases the spatial resolution of the shear map, which eventually washes out shear produced by substructures.

2. This limitation can be overcome by ultra-deep images which provide a large number of galaxies on small areas. Unfortunately, because these objects are so faint, their centroid and their shape parameters can be determined only poorly from observation. Furthermore, deep HST images show that

Key words: dark matter – gravitational lensing – observational methods – clusters of galaxies – quasars: 2345+007 – clusters of galaxies: 0024+16

1. Introduction

Weak gravitational lensing is one of the most promising tools for probing the amount and the distribution of mass in the universe. The small anisotropy in the shape of galaxies induced

Send offprint requests to:

a large fraction of the faintest galaxies have no well-defined shapes and show many bright spots which can be mistakenly considered as galaxy centroids on ground based images.

In this paper we propose an alternative method for the shear measurement which can overcome these critical issues. Such a method, which uses the auto-correlation function of the brightness distribution (hereafter ACF) of the *whole* image, was implemented by some authors (Cole et al. 1992, Dalcanton 1996) to detect small amplitude variations in the mean noise associated with faint cluster of galaxies. The philosophy of the correlation methods is to avoid individual object detection in order to work at the noise limit, and consequently to go much deeper than classical analyses. Here, the fundamental point is that a stretching of a shear-free image by gravitational distortion induces an equivalent stretching in the auto-correlation function. The strong advantage is that the co-addition is made without computation of the central moments of individual objects, and, as shown later, the signal-to-noise of the ACF can be greater than a direct co-addition of the objects. In fact, the concept of object itself is no more relevant: the CCD field is viewed as a fluctuating ‘density field’, and the objects are viewed as ‘overdensities’. Consequently, any overdensity present on the CCD, even if it is related to extremely faint sources which have not been detected with standard detection algorithms, provides information about the ACF. For that reason, the faintest sources, which only emerge from the noise limit of the background, will be detected by the ACF. It will provide additional information of the shear field from the modification of the noise pattern which, as a result, appears as a “*sheared noise pattern*”.

Obviously, the signal-to-noise ratio of the ACF depends on the number density of faint background sources. The most recent deep galaxy counts in the visible at the Keck telescope (Smail et al. 1995) yields compelling evidence that the ACF should be considerably more powerful than the standard method. Consider for instance a standard detection criterium based on the positive measurement of a connex-shape object formed with at least 6 pixels at least one σ (standard deviation) above the background. In practice, this definition rejects smaller objects with flux per pixel larger than two σ above the background because they look like cosmic ray events (steep slope of the contours). Therefore, the largest “undetected” pattern which could be a galaxy in the CCD may have 5 pixels, having at most one σ above the background. From our own observational data obtained at the Canada-France-Hawaii Telescope (CFHT), this “undetected” pattern corresponds to objects with magnitude $V = 30.4$ on a 5 hours exposure. Extrapolating the deep galaxy counts of Smail et al. (1995) we expect about 2×10^6 gal./deg²/mag. at $V = 30.4$, or about 550 gal./arcmin²/mag.! In our CCD field this amounts to about one object per field of 5 arcsec²! The ACF method will take into account any of these ultra-faint galaxies without the need to determine their individual position and shape. We therefore expect a considerable increase of the signal. Conversely, we may use the increase of the signal-to-noise ratio on the shear to analyse the projected number density of these ultra-faint sources.

In this first paper we only discuss the implication of the ACF technique for the (weak) shear measurement. The analysis of the background population is discussed in a forthcoming paper (Van Waerbeke et al.; Paper II). In the next section, we present the basic formalism and demonstrate how the ACF

is “gravitationally distorted” by the shear. We show that the ACF method is strictly equivalent to a single object analysis but with a high signal-to-noise ratio. The third section shows how to extract the gravitational shear information from the ACF. In particular, we present a detailed analysis of the error estimation. The fourth section validates the method on simulated data and on real images from which we know the shear pattern from the standard detection technique (BMF). There, we compare shear maps obtained from the auto-correlation function with those measured by the ‘standard method’ for the double QSO 2345+007 and for the inner part and an outer region of the cluster Cl 0024+16 and show that these shear maps are in excellent agreement.

2. The Auto-correlation Method

2.1. The basic formalism

Throughout this paper we keep solely a geometrical point of view of the shear effects. This means that we do not consider the mass reconstruction problem.

Consider a gravitational lens at some redshift z_d which is sufficiently small such that the distance of all sources can be approximately set to a constant (or more precisely, the distance ratio D_{ds}/D_s is the same for all sources). In a solid angle which is sufficiently small such that the local lensing properties do not change over this region, the lens equation can be locally linearized, such that the angle β of a light ray in the ‘source plane’ is related to its observed angular position in the lens plane by

$$\beta = \beta_0 + A(\theta_0)(\theta - \theta_0) \quad (1)$$

where θ_0 is a central position of the angular region considered, β_0 the corresponding angular position in the source plane, and A is the local Jacobian matrix, which reads

$$A = \begin{pmatrix} 1 - \kappa - \gamma_1 & -\gamma_2 \\ -\gamma_2 & 1 - \kappa + \gamma_1 \end{pmatrix} \equiv (1 - \kappa)\mathcal{I} - \gamma J(\varphi) \quad (2)$$

where κ is the local dimensionless surface mass density, γ_i , $i = 1, 2$, are the two components of the shear (for more details, see Schneider, Ehlers & Falco 1992), \mathcal{I} is the two-dimensional identity matrix, and

$$J(\varphi) = \begin{pmatrix} \cos 2\varphi & \sin 2\varphi \\ \sin 2\varphi & -\cos 2\varphi \end{pmatrix} \quad (3)$$

is a symmetric traceless tensor which describes the orientation φ of the shear. Conservation of surface brightness implies that the observed surface brightness $I(\theta)$ is related to the intrinsic one $I^{(s)}(\beta)$ by

$$I(\theta) = I^{(s)}(A\theta) \quad (4)$$

where we have applied a translation of the coordinates in the source plane to remove the constant terms in (1); this can be done since absolute positions in the source plane are unobservable anyway.

We now define the auto-correlation function of the brightness in the image plane by

$$\xi(\theta) = \langle (I(\theta) - \bar{I})(I(\theta + \theta) - \bar{I}) \rangle_{\theta} \quad (5)$$

where the angular brackets denote an average over all positions $\boldsymbol{\vartheta}$, and \bar{I} is the mean surface brightness of the image. Inserting the relation (4) into (5), one finds immediately that

$$\xi(\boldsymbol{\theta}) = \xi^{(s)}(A\boldsymbol{\theta}) \quad (6)$$

where the auto-correlation function $\xi^{(s)}$ is defined in analogy to (5) with I replaced by $I^{(s)}$. Hence we see that the ‘observed’ correlation function ξ is related in a simple way to the ‘intrinsic’ one. In particular, the intrinsic correlation function can be assumed to be isotropic; then (6) shows that the observed correlation function will in general be anisotropic. The power spectrum of the surface brightness, defined as the square of the Fourier-transform $\hat{\xi}(\mathbf{k})$ of the correlation function, is related to the intrinsic power spectrum by

$$|\hat{\xi}(\mathbf{k})|^2 = \mu^2 |\hat{\xi}^{(s)}(A^{-1}\mathbf{k})|^2 \quad (7)$$

where $\mu = 1/\det A$ is the local magnification of the lens.

If the intrinsic correlation function $\xi^{(s)}(\boldsymbol{\beta})$ is known, the relation (6) allows to determine the local Jacobian matrix A , and thus the shear components γ and surface mass density κ (note that this is not strictly true if the lensing is not ‘weak’, as will be discussed later). We shall return to the practical questions concerning this issue further below. However, even if the intrinsic correlation function is unknown, but only assumed to be isotropic (which should be a very good approximation), one can obtain some information on the Jacobian matrix A , as we show next.

Consider the tensor of second moments of the auto-correlation function,

$$\mathcal{M}_{ij} = \frac{\int d^2\theta \xi(\boldsymbol{\theta}) \theta_i \theta_j}{\int d^2\theta \xi(\boldsymbol{\theta})} \quad (8)$$

and the corresponding definition for the tensor $\mathcal{M}_{ij}^{(s)}$ of second moments of the intrinsic auto-correlation function; using the relation (6), one readily obtains

$$\mathcal{M}_{ij} = A_{ik}^{-1} A_{jl}^{-1} \mathcal{M}_{kl}^{(s)} \quad (9)$$

an equation very similar to the transformation of second brightness moments of individual galaxy images (e.g., Blandford et al. 1991, Schneider & Seitz 1995, BM). The main formal difference is that individual galaxies cannot be assumed to be isotropic in the source plane, so that the observed ellipticity of a galaxy image depends on both, the Jacobian matrix *and* the intrinsic source ellipticity. In the case considered here, $\mathcal{M}_{ij}^{(s)}$ can be considered an isotropic tensor, so that

$$\mathcal{M}_{ij}^{(s)} = \frac{1}{2} \frac{\int d\beta \beta^3 \xi^{(s)}(\boldsymbol{\beta})}{\int d\beta \beta \xi^{(s)}(\boldsymbol{\beta})} \delta_{ij} \equiv M \delta_{ij} \quad (10)$$

where we have defined the mean quadratic radius M of the intrinsic correlation function in the second step. Inserting (10) into (9) and using the form (2) of the matrix A , one finds after some algebra

$$\mathcal{M} = \frac{M}{(1-\kappa)^2 (1-|g|^2)^2} \times \begin{pmatrix} 1+2g_1+|g|^2 & 2g_2 \\ 2g_2 & 1-2g_1+|g|^2 \end{pmatrix} \quad (11)$$

where we have defined the *reduced shear*

$$g_i := \frac{\gamma_i}{(1-\kappa)}. \quad (12)$$

We shall see that it is convenient to also introduce the *distortion*

$$\delta_i := \frac{2g_i}{(1+|g|^2)}, \quad (13)$$

which has also been used in weak lensing studies before (e.g., Miralda-Escudé 1991, Schneider & Seitz 1995, BM). With this definition, (11) can also be written as

$$\mathcal{M} = \frac{M(1+|g|^2)}{(1-\kappa)^2 (1-|g|^2)^2} \begin{pmatrix} 1+\delta_1 & \delta_2 \\ \delta_2 & 1-\delta_1 \end{pmatrix}. \quad (14)$$

From the latter form, one can immediately read off that

$$\delta_1 = \frac{\mathcal{M}_{11} - \mathcal{M}_{22}}{\text{tr}\mathcal{M}}, \quad \delta_2 = \frac{2\mathcal{M}_{12}}{\text{tr}\mathcal{M}}, \quad (15)$$

where $\text{tr}\mathcal{M} = \mathcal{M}_{11} + \mathcal{M}_{22}$ is the trace of \mathcal{M} . Furthermore, from the trace of (14), one obtains

$$(1-\kappa)^2 = \frac{M}{4\det\mathcal{M}} (\text{tr}\mathcal{M} \pm 2\sqrt{\det\mathcal{M}}). \quad (16)$$

In order to appreciate this solution, the corresponding situation for the determination of lensing parameters from individual galaxy images should be recalled: there, using only the shape of the galaxy images, together with the assumption that the intrinsic orientation of galaxies is randomly distributed, the distortion δ can be uniquely determined. Furthermore, the local magnification can in principle be obtained, either from changes of the local number density of background galaxy images due to the magnification (anti-)bias (Broadhurst, Taylor & Peacock 1995), or by changes of the image sizes at fixed surface brightness (Bartelmann & Narayan 1995). The same information can be obtained in the situation under consideration here: the distortion can be uniquely determined (15) from assuming that the intrinsic correlation function is isotropic, without knowledge of its radial dependence, whereas the (absolute value of the) magnification

$$|\mu| = \frac{\sqrt{\det\mathcal{M}}}{M} \quad (17)$$

can be determined if the second moment of the intrinsic correlation M function is known. Note that a given combination of δ and $|\mu|$ does not specify the shear γ and local surface mass density κ uniquely; in fact, for each such combination, four different pairs of (γ, κ) are obtained, corresponding to the four different combinations of $(\mu > 0, \mu < 0)$ and $(\kappa < 1, \kappa > 1)$. Only one of these combinations, $\mu > 0, \kappa < 1$, is relevant for non-critical clusters, or the region outside the critical curves in critical clusters.

We can now consider the case of weak lensing, i.e., $\kappa \ll 1$, $|\gamma| \ll 1$. Assuming again that the intrinsic correlation function is isotropic, $\xi^{(s)}(\boldsymbol{\beta}) = \xi^{(s)}(|\boldsymbol{\beta}|)$, we can expand (6) to obtain

$$\xi(\boldsymbol{\theta}) \approx \xi^{(s)}(\theta) - \theta \xi^{(s)'}(\theta) [\kappa + \gamma J(\varphi - \vartheta)], \quad (18)$$

where we have written $\boldsymbol{\theta} = \theta(\cos \vartheta, \sin \vartheta)$. Equation (18) shows, in the case of weak lensing, that the observed correlation function is the sum of the intrinsic correlation function and a perturbative term which linearly depends on both κ and γ .

2.2. Inclusion of a point spread function

Equation (4) is only an idealized description of the brightness distribution obtained from observations; in practice, it is affected by observational effects (seeing, tracking errors, etc.) and noise. We consider the first of these effects here, and assume that it can be described by a point spread function (PSF) $W(\boldsymbol{\psi})$ which is taken to be normalized,

$$\int d^2\boldsymbol{\psi} W(\boldsymbol{\psi}) = 1. \quad (19)$$

The observed brightness profile $I^{(\text{obs})}(\boldsymbol{\theta})$ is then given by

$$\begin{aligned} I^{(\text{obs})}(\boldsymbol{\theta}) &= \int d^2\boldsymbol{\psi} W(\boldsymbol{\theta} - \boldsymbol{\psi}) I(\boldsymbol{\psi}) \\ &= \int d^2\boldsymbol{\psi} W(\boldsymbol{\theta} - \boldsymbol{\psi}) I^{(\text{s})}(A\boldsymbol{\psi}). \end{aligned} \quad (20)$$

This observed brightness profile can now be inserted into the definition (5) to obtain the observed correlation function $\xi^{(\text{obs})}(\boldsymbol{\theta})$, for which one obtains

$$\begin{aligned} \xi^{(\text{obs})}(\boldsymbol{\theta}) &= \int d^2\boldsymbol{\psi} T(\boldsymbol{\theta} - \boldsymbol{\psi}) \xi(\boldsymbol{\psi}) \\ &= \int d^2\boldsymbol{\psi} T(\boldsymbol{\theta} - \boldsymbol{\psi}) \xi^{(\text{s})}(A\boldsymbol{\psi}), \end{aligned} \quad (21)$$

where the self-convolved PSF T is given by

$$T(\boldsymbol{\theta}) = \int d^2\boldsymbol{\psi} W(\boldsymbol{\theta} - \boldsymbol{\psi}) W(\boldsymbol{\psi}); \quad (22)$$

as can be easily seen, the normalization of W implies that T is also normalized.

In analogy to the definition (8), one can now define the tensor $\mathcal{M}_{ij}^{(\text{obs})}$ of second moments of the observed auto-correlation function; using Eq. (21), one finds that

$$\mathcal{M}_{ij}^{(\text{obs})} = \mathcal{M}_{ij} + \mathcal{T}_{ij}, \quad (23)$$

where

$$\mathcal{T}_{ij} := \int d^2\boldsymbol{\theta} T(\boldsymbol{\theta}) \theta_i \theta_j \quad (24)$$

is the tensor of second moments of the self-convolved PSF. Hence, provided the PSF can be obtained with sufficient accuracy, the tensor \mathcal{M}_{ij} can be directly obtained from (23), and thus the distortion δ and magnification $|\mu|$ can be determined from (15) and (17) as before. The accuracy with which \mathcal{M}_{ij} can be obtained depends of course on the accuracy with which $T(\boldsymbol{\psi})$ is known, as well as on the relative ‘size’ of \mathcal{M} and \mathcal{T} ; if the components of \mathcal{T} are much larger than those of \mathcal{M} , the determination of $\mathcal{M} = \mathcal{M}^{(\text{obs})} - \mathcal{T}$ involves subtraction of two ‘big numbers’ and is thus subject to large fractional errors.

If the PSF is isotropic, so is T ; in this case, we can then write for the tensor $\mathcal{T}_{ij} = T\delta_{ij}$. The distortion and magnification in terms of $\mathcal{M}^{(\text{obs})}$ is then given by

$$\begin{aligned} \delta_1 &= \frac{\mathcal{M}_{11}^{(\text{obs})} - \mathcal{M}_{22}^{(\text{obs})}}{\text{tr}\mathcal{M}^{(\text{obs})} - 2T}, \\ \delta_2 &= \frac{2\mathcal{M}_{12}^{(\text{obs})}}{\text{tr}\mathcal{M}^{(\text{obs})} - 2T}, \\ |\mu| &= \frac{\sqrt{\det\mathcal{M}^{(\text{obs})} - T\text{tr}\mathcal{M}^{(\text{obs})} + T^2}}{M}. \end{aligned} \quad (25)$$

2.3. Practical estimate of the distortion

2.3.1. Estimates neglecting a PSF

The calculation of the tensor \mathcal{M} of second moments of the correlation function according to (8) is impossible in practice, since the integral extends over the whole \mathbb{R}^2 , and therefore will be dominated by noise. One would like to have the integral extend over a finite region only. Here, we outline several possibilities how, despite this difficulty, the distortion δ can be determined.

Adding a weight factor $w_\theta(|\boldsymbol{\theta}|)$ in the integrals in the definition (8),

$$\mathcal{M}_{ij} = \frac{\int d^2\boldsymbol{\theta} \xi(\boldsymbol{\theta}) \theta_i \theta_j w_\theta(|\boldsymbol{\theta}|)}{\int d^2\boldsymbol{\theta} \xi(\boldsymbol{\theta}) w_\theta(|\boldsymbol{\theta}|)}, \quad (26)$$

would destroy the transformation relation (9), since this isotropic weight function would correspond to an anisotropic weight function in the source plane. However, the weight function $w_\theta(|\boldsymbol{\theta}|)$ could be chosen to be about zero for small values of $|\boldsymbol{\theta}|$ to minimize the PSF pollution, and also for large value when ξ approaches the noise level. In particular, the distortion can be determined without any knowledge about the intrinsic correlation function $\xi^{(\text{s})}$, except that it is assumed to be isotropic. This is the method we choose for the practical implementation of the ACF method in the next Section.

Another possibility is to define the tensor of second moments as a function of the Jacobian matrix; for that we note that we can write the Jacobian as $A = aB$, where

$$B = \begin{pmatrix} 1 + \sqrt{1 - |\delta|^2} - \delta_1 & -\delta_2 \\ -\delta_2 & 1 + \sqrt{1 - |\delta|^2} + \delta_1 \end{pmatrix}, \quad (27)$$

and a is a scalar. We now define the δ -dependent moment matrix

$$\bar{\mathcal{M}}_{ij} = \frac{\int d^2\boldsymbol{\theta} \xi(\boldsymbol{\theta}) \theta_i \theta_j w^{(\text{s})}(|B\boldsymbol{\theta}|)}{\int d^2\boldsymbol{\theta} \xi(\boldsymbol{\theta}) w^{(\text{s})}(|B\boldsymbol{\theta}|)}, \quad (28)$$

where $w^{(\text{s})}(x)$ is a weight function. Note that this matrix now explicitly depends on δ , and can be calculated from the observed correlation function for each value of δ . Changing the integration variable to $\boldsymbol{\beta} = A\boldsymbol{\theta} = aB\boldsymbol{\theta}$, one finds that

$$\bar{\mathcal{M}}^{(\text{s})} = A\bar{\mathcal{M}}A = a^2 B\bar{\mathcal{M}}B, \quad (29)$$

where the matrix

$$\bar{\mathcal{M}}_{ij}^{(\text{s})} = \frac{\int d^2\boldsymbol{\beta} \xi^{(\text{s})}(\boldsymbol{\beta}) \beta_i \beta_j w^{(\text{s})}(|\boldsymbol{\beta}|/a)}{\int d^2\boldsymbol{\beta} \xi^{(\text{s})}(\boldsymbol{\beta}) w^{(\text{s})}(|\boldsymbol{\beta}|/a)} \quad (30)$$

is defined in analogy to (28). What is important to note is that the isotropy of $\xi^{(\text{s})}$ implies that $\bar{\mathcal{M}}^{(\text{s})}$ is again an isotropic matrix. In other words, the expression

$$\nu := \frac{(\bar{\mathcal{M}}_{11}^{(\text{s})} - \bar{\mathcal{M}}_{22}^{(\text{s})})^2 + 4(\bar{\mathcal{M}}_{12}^{(\text{s})})^2}{(\bar{\mathcal{M}}_{11}^{(\text{s})} + \bar{\mathcal{M}}_{22}^{(\text{s})})^2} \quad (31)$$

should vanish. If $\bar{\mathcal{M}}^{(\text{s})}$ is replaced by the observed tensor $\bar{\mathcal{M}}$ using Eq. (29), ν will not vanish in general, unless the correct value for δ was chosen. Performing this substitution, we find

$$\nu(\delta) = 1 - \frac{4\det\bar{\mathcal{M}}(1 - |\delta|^2)}{[\text{tr}\bar{\mathcal{M}} - \delta_1(\bar{\mathcal{M}}_{11} - \bar{\mathcal{M}}_{22}) - 2\delta_2\bar{\mathcal{M}}_{12}]^2}; \quad (32)$$

note that the scalar factor a drops out. Thus, ν depends on δ explicitly, as well as through the dependence of $\bar{\mathcal{M}}$ on δ . Since ν is positive semi-definite, a minimization of ν will determine the value of δ .

To summarize the basic idea of this approach, the weight function in the definition of the second moment tensor is chosen such as to yield an isotropic weight factor *in the source plane*, and it is adjusted such that the tensor of second moments in the source plane, as calculated from the observed tensor and the transformation (31), becomes isotropic. The weight function $w^{(s)}$ will be chosen such that it decreases to zero at radii where the signal-to-noise of the observed correlation function reaches about unity; for example, $w^{(s)}$ could be a Gaussian, with width adjusted to the data quality.

2.3.2. Inclusion of a PSF

If the effects of a PSF are included, together with a weighting scheme, the transformation becomes much more complicated than the one in (23). Hence, as was the case for the estimate of the distortion from galaxy images, the analysis becomes considerably more complicated if the effects of a PSF are taken into account (BM; Kaiser, Squires & Broadhurst 1995). The most serious effect is the gradual deterioration of the ‘isophote’ shape toward the ACF center. An issue to this problem is to use simulated images to calibrate the PSF effect on the shape of the objects as described in BM. We choose this method conjointly to the biased weighting scheme (Eq. 26) instead of the unbiased Eq. (28). The reason is that for real data, the ACF is generally too noisy to allow a good shape parameter estimation from the intensity weighted formula given by Eq. (28).

Since the signal-to-noise of the observed correlation function $\xi^{(\text{obs})}$ can be quite large, compared to single faint galaxy images, it might be worthwhile to use an ‘image restoration technique’ to invert the relation (21) between the observed correlation function $\xi^{(\text{obs})}$ and the true one, ξ . From the result of this restoration process (which could be, e.g., the Lucy 1994 algorithm), the tensor $\bar{\mathcal{M}}$ can be calculated and the method outlined above can be used. Obviously, the result will not only depend on the quality of the data $\xi^{(\text{obs})}$, but critically on the knowledge of the (local) PSF, or more precisely, its self-convolved form T . Unfortunately, the image restoration technique has not given satisfactory result in the cases we have tested, and we will not pursue this idea further here. However, we think that it should be kept in mind and analysed in more detail.

There might be a better way for the determination of the distortion (and the local magnification) in the presence of a PSF. The correlation $\xi^{(s)}$ is due to very many faint galaxy images if the brighter objects are removed (see below). Therefore, one might hope that this intrinsic correlation function $\xi^{(s)}$ is a universal function, being the same in all directions. Such a source correlation function will be obtainable from the Deep HST survey. If that were true, one would have a ‘standard source’ at high redshifts, and it is no surprise that that would help the analysis considered here tremendously. To wit, in this case one could compare the observed correlation function $\xi^{(\text{obs})}$ with the one calculated from the PSF and the intrinsic correlation function $\xi^{(s)}$, i.e., one can define

$$\chi^2 = \sum_k \frac{[\xi^{(\text{obs})}(\boldsymbol{\theta}_k) - \int d^2\boldsymbol{\psi} T(\boldsymbol{\theta}_k - \boldsymbol{\psi}) \xi^{(s)}(|A\boldsymbol{\psi}|)]^2}{\sigma_k^2}, \quad (33)$$

where the sum extends over all values (pixels) on which the correlation function $\xi^{(\text{obs})}$ is determined, and σ_k is the standard deviation of the value of $\xi^{(\text{obs})}$ at $\boldsymbol{\theta}_k$. By minimizing χ^2 , the matrix A can be determined. As has become clear from the discussion at the end of Sect. 2.1, κ and γ cannot be determined observationally, but the quantities which can be determined are δ and $|\mu|$. Hence, for the use in (33), one should parametrize the matrix A as

$$A \doteq \frac{1}{\sqrt{2|\mu|(1 - |\delta|^2 + \sqrt{1 - |\delta|^2})}} \times \begin{pmatrix} 1 + \sqrt{1 - |\delta|^2} - \delta_1 & -\delta_2 \\ -\delta_2 & 1 + \sqrt{1 - |\delta|^2} + \delta_1 \end{pmatrix}, \quad (34)$$

where the symbol ‘ \doteq ’ implies that the right-hand side is equal to A only in the non-critical regime, but that in the critical regime, the equivalent form of A in terms of $|\mu|$ and δ is the same as in (34). Thus, if the intrinsic correlation function is known, one can determine $|\mu|$ and δ by inserting the form (34) for A into (33) and minimizing χ^2 with respect to $|\mu|$ and the two components of δ .

3. Practical estimation in the weak-shear limit, and error analysis

3.1. The practical method

3.1.1. Practical estimate of the correlation function

Up to now we have considered a lens mapping which can be described by its linearized form (1) over a sufficiently large solid angle in the sky. In practice, if one observes a cluster of galaxies, the linearization of the lens mapping will be valid only locally, on scales small compared to the typical angular scale on which the surface mass density of the cluster varies significantly. In those cases, one is interested in obtaining local estimates for the distortion and the surface mass density, i.e., the average in (5) should be extended over a limited area only. For our task, in order to avoid boundary effects of Fourier transforms in finite size fields, we choose to compute the ACF from the direct method which is more CPU time consuming than the Fourier analysis, but more accurate. In addition, the observational frame contains bright objects, such as foreground stars, cluster galaxies, or bright field galaxies which would dominate the obtained correlation function if not removed of the average in (5). Taking these difficulties into account, we propose a practical estimator for the determination of the local correlation function.

Let \mathcal{U} denote the frame on which data are available. The bright objects can be identified and ‘cut out’. This is done by using the FOCAS package to select the bright objects and replace them by a shaded area. It is important to note here that this shaded area does not bias the estimate of the ACF, provided it is not included in the ACF computation. The selection criteria must be such that the bright objects are completely covered by the shade mask. The resulting frame after cutting out these patches will have a ‘Swiss cheese’ shape and will be denoted by \mathcal{U}' afterwards. On this field \mathcal{U}' , one then defines the

mean intensity (in this section, we drop the superscript ‘obs’ for the observed intensity and correlation function)

$$\bar{I} = \frac{1}{N'} \sum_{k \in \mathcal{U}'} I_k, \quad (35)$$

where the sum extends over all the N' pixels in \mathcal{U}' , and the intensity deviations $i_k = I_k - \bar{I}$. From that, the correlation function of brightness fluctuations at position $\boldsymbol{\theta}_0$ is defined as

$$\xi(\boldsymbol{\theta}; \boldsymbol{\theta}_0) = \frac{\sum_{\boldsymbol{\psi}} i(\boldsymbol{\psi} - \boldsymbol{\theta}/2) i(\boldsymbol{\psi} + \boldsymbol{\theta}/2) w(|\boldsymbol{\psi} - \boldsymbol{\theta}_0|)}{\sum_{\boldsymbol{\psi}} w(|\boldsymbol{\psi} - \boldsymbol{\theta}_0|)}, \quad (36)$$

where the sums in numerator and denominator are taken over all possible values of $\boldsymbol{\psi}$ such that $\boldsymbol{\psi} \pm \boldsymbol{\theta}/2$ both lie in \mathcal{U}' , and $w(\theta)$ is a weight function, typically chosen to be a Gaussian of width $\Delta\theta$. $\xi(\boldsymbol{\theta}; \boldsymbol{\theta}_0)$ is often named Energy of the image \mathcal{U}' . Hence, the expression (36) defines the correlation function as the weighted average over products of pairs of points with separation vector $\boldsymbol{\theta}$ which can be selected within \mathcal{U}' , and the contribution to the average is weighted by the function w which depends on the separation of the midpoint of the pair from the point $\boldsymbol{\theta}_0$ at which the correlation function is calculated.



Fig. 1. A characteristic auto-correlation pattern at the faint galaxy angular scale. The ACF is computed from a 256×256 superpixel of the I band of Q2345. Note in the central part of the ACF a crux pattern. This is a possible consequence of the loss of Charge Transfer Efficiency and/or the shift and add procedure.

An example of a correlation function is shown in Figure 1. Only the central part of the ACF (40×40 pixels) is represented. The rest of the image contains noise plus interference terms which correspond to the overlapping of a galaxy by another galaxy. These cross-correlation terms are irrelevant for our purpose.

3.1.2. Second moment measurement

Eq. (21) shows that the observed ACF is a convolution of the true ACF with the square of the PSF, which is $\sqrt{2}$ times larger

than the PSF for a gaussian shape. No information is lost since the true ACF is also $\sqrt{2}$ times larger than a typical galaxy size. However, this effect must be taken into account for the computation of the moments of the ACF, in particular for the choice of the filter. As pointed out by BM, the usual way to estimate the second moments of an object within a limiting isophote is not ideal. The convolution by the PSF changes the shapes of the isophotes which become nearly circular in the center of the object with little information left on the gravitational shear. The best way to estimate \mathcal{M}_{ij} seems to use an annular weighting function $w_{\theta}(\boldsymbol{\theta})$ centered on the ACF. Note that, contrary to the case of individual galaxies, the center of the ACF is, by definition, perfectly known. Since most of the gravitational shear signal is extending between 1 and 2 seeing disks around the center of a galaxy, a natural choice for w_{θ} is:

$$w_{\theta}(\boldsymbol{\theta}) = e^{-(\theta/s)^2+1} e^{-(s/\theta)^2+1} \quad (37)$$

where s is the angular size of the seeing disk. The shear $\gamma = |\gamma|e^{2i\varphi}$ thus inferred must be corrected. Indeed, the magnitude $|\gamma|$ is underestimated due to the use of the weighting function w_{θ} , and to the PSF convolution.

The problem of this underestimation was discussed earlier by several authors, as in BM, Fahlman et al. (1994), and Kaiser, Squires & Broadhurst (1995). BM concluded that this effect can be corrected using simulations from which they calibrate the measured shear intensity to the true one. They showed that the measured shear intensity is simply proportional to the true one (provided that the weak shear approximation applies). Fahlman et al. showed that the calibration constant can be found from a stretching of the images and convolving them with a known and large isotropic PSF. Kaiser et al. proposed to use HST images, stretch them by a known shear, reconvolve them with a PSF typical for ground-based observations, and then compare the resulting value of the measured ‘shear’ with the input value to obtain the correction factor between true and observed shear.

As in BM, we choose here to use simulated images for the calibration. However, HST images provide an elegant way to calibrate the effect, as quoted in Section 2.3.2, but this requires a deep ‘empty field’, and will be done in further work.

3.2. Errors coming from the noise level of the ACF

This Section is devoted to the error measurement coming from the noisy aspect of the ACF. This is an important issue: contrary to standard methods where the shear is inferred from the averaged shapes of many galaxies, the ACF method gives ultimately the shape of only one object, the ACF itself. It is therefore crucial to properly quantify the various sources of noise.

In the first subsection, the signal-to-noise ratio of the ACF (S/N) is expressed in terms of the galaxy number N_g , the field size, and the S/N of the individual galaxies, called σ_0 . The second subsection quantifies the dependence of the shear measurement on the S/N of the ACF.

3.2.1. Dependence of the S/N of the ACF on the image parameters

To simplify the discussion, assume that the image contains N'_g galaxies having the same size, the same profile, and the same surface brightness. We can then write the surface brightness as

$I(\boldsymbol{\theta}) = I_{\text{sky}} + i_n(\boldsymbol{\theta}) + \sum_{k=1}^{N'_g} I_g(\boldsymbol{\theta} - \boldsymbol{\theta}_k)$, where I_{sky} is the sky brightness, $i_n(\boldsymbol{\theta})$ are the brightness fluctuations, and the third term is the contribution from the galaxies, situated at positions $\boldsymbol{\theta}_k$, with brightness profile I_g . Subtracting the mean \bar{I} from $I(\boldsymbol{\theta})$, one obtains that $i(\boldsymbol{\theta}) = \sum_{k=1}^{N'_g} I_g(\boldsymbol{\theta} - \boldsymbol{\theta}_k) - \bar{I}_g + i_n(\boldsymbol{\theta}) \equiv \sum_{k=1}^{N'_g} \hat{I}_g(\boldsymbol{\theta} - \boldsymbol{\theta}_k) + i_n(\boldsymbol{\theta})$, where \bar{I}_g is the mean brightness contributed by the galaxies. Since the galaxies are faint, and we are far from the confusion limit, practically all photons can be attributed to the sky brightness, which implies that the noise $i_n(\boldsymbol{\theta})$ is Poisson noise almost entirely due to the sky brightness photons, i.e., $\sigma_{\text{sky}}^2 \equiv \langle i_n^2(\boldsymbol{\theta}) \rangle = I_{\text{sky}}$, if intensities are measured in photon numbers. In particular, this means that the noise is uncorrelated with the signal.

Inserting the foregoing expression for $i(\boldsymbol{\theta})$ into (36), one finds that

$$\begin{aligned} \xi(\boldsymbol{\theta}; \boldsymbol{\theta}_0) &= \frac{1}{\sum_{\psi} w(|\boldsymbol{\psi} - \boldsymbol{\theta}_0|)} \sum_{\psi} w(|\boldsymbol{\psi} - \boldsymbol{\theta}_0|) \\ &\times \left[i_n(\boldsymbol{\psi} - \boldsymbol{\theta}/2) i_n(\boldsymbol{\psi} + \boldsymbol{\theta}/2) \right. \\ &+ i_n(\boldsymbol{\psi} - \boldsymbol{\theta}/2) \sum_{k=1}^{N'_g} \hat{I}_g(\boldsymbol{\psi} + \boldsymbol{\theta}/2 - \boldsymbol{\theta}_k) \\ &+ i_n(\boldsymbol{\psi} + \boldsymbol{\theta}/2) \sum_{k=1}^{N'_g} \hat{I}_g(\boldsymbol{\psi} - \boldsymbol{\theta}/2 - \boldsymbol{\theta}_k) \\ &\left. + \sum_{j=1}^{N'_g} \hat{I}_g(\boldsymbol{\psi} - \boldsymbol{\theta}/2 - \boldsymbol{\theta}_j) \sum_{k=1}^{N'_g} \hat{I}_g(\boldsymbol{\psi} + \boldsymbol{\theta}/2 - \boldsymbol{\theta}_k) \right] \quad (38) \end{aligned}$$

One thus sees that ξ contains contributions from galaxies only, from products of galaxy brightness and the noise, and terms proportional to the square of the noise. Considering $\boldsymbol{\theta} \neq \mathbf{0}$, then the fact that the noise in different pixels is uncorrelated, and that the noise is uncorrelated with the signal contributed by the galaxies implies that the expectation value of ξ is determined by the final term in (38). This can be split up into terms with $j = k$, and in those with $j \neq k$. The former thus contain the ACF of the galaxy brightness profiles and its result is proportional to N'_g . The latter contains cross-correlations of different galaxies, and is proportional to $N'_g{}^2$ times the two-point angular correlation function of galaxy positions.

More precisely, if we define the auto-correlation function of an individual galaxy as

$$\xi_g(\boldsymbol{\theta}) = \int d^2\vartheta \hat{I}_g(\boldsymbol{\vartheta} - \boldsymbol{\theta}/2) \hat{I}_g(\boldsymbol{\vartheta} + \boldsymbol{\theta}/2), \quad (39)$$

and neglect the possible angular correlation of galaxy positions [i.e., the terms with $j \neq k$ in the last term in (38)], then one finds that the expectation value $\langle \xi(\boldsymbol{\theta}; \boldsymbol{\theta}_0) \rangle$ of the ACF becomes

$$\langle \xi(\boldsymbol{\theta}; \boldsymbol{\theta}_0) \rangle = \frac{\sum_{j=1}^{N'_g} w(|\boldsymbol{\theta}_j - \boldsymbol{\theta}_0|)}{\sum_{\psi} w(|\boldsymbol{\psi} - \boldsymbol{\theta}_0|)} \xi_g(\boldsymbol{\theta}), \quad (40)$$

provided the weight function $w(\boldsymbol{\theta})$ does not vary on scales comparable to the size of individual galaxies. Correspondingly, the noise in the ACF becomes

$$\sqrt{\langle [\xi - \langle \xi(\boldsymbol{\theta}; \boldsymbol{\theta}_0) \rangle]^2 \rangle} = \sigma_{\text{sky}}^2 \frac{\sqrt{\sum_{\psi} w^2(|\boldsymbol{\psi} - \boldsymbol{\theta}_0|)}}{\sum_{\psi} w(|\boldsymbol{\psi} - \boldsymbol{\theta}_0|)}. \quad (41)$$

For the special case of a rectangular top-hat filter with $N_x \times N_y$ pixels, centered on $\boldsymbol{\theta}_0$, the corresponding signal-to-noise ratio of the ACF becomes

$$S/N = \frac{N_g}{\sqrt{N_x N_y}} \frac{\xi_g(\boldsymbol{\theta})}{\sigma_{\text{sky}}^2}, \quad (42)$$

where now N_g is the number of galaxies contained in the top-hat filter. We thus see that the signal-to-noise ratio is proportional to the number of galaxies within the filter. This should be contrasted to the case where the shear is determined from individual galaxy images; in that case, the signal-to-noise increases only as the square root of N_g . This fact shows that the ACF method will be superior to the standard method if the number (density) of galaxies is sufficiently high. Furthermore, S/N depends on the filter scale, or in other words, depends on the number density n of the galaxies, $S/N \propto n \sqrt{N_x N_y}$.

The S/N also depends on the flux of the individual galaxies. This is a consequence of the fact that, by definition, the objects in the ACF are weighted by the square of their flux [see Eq. (36)]. Therefore the S/N increases as the square of the flux of the individual galaxies; that is as σ_0^2 .

In this simple discussion where we neglected the profiles and the sizes of individual galaxies, we can therefore express S/N as follows:

$$\frac{S}{N} = K \sqrt{\frac{256 \times 256}{N_x N_y}} N_g \sigma_0^2. \quad (43)$$

The constant K can be determined from the profile and size of individual galaxies; here, we obtain it from the hypothesis that all the galaxies have the same size, profile and flux. They are modeled by a gaussian profile of diameter 5 pixels. We define the S/N of an object (ACF or galaxy) as the mean amplitude of the object in an annulus of radius 3 pixels with a width of 1 pixel centered on the object, divided by the sky photon noise. As explained in Section 3.1.2, the inner and outer radii of the annulus are justified by the fact that we avoid the central part of the object which is strongly polluted by the PSF.

With these definitions, and for a square-shaped two-dimensional top-hat filter w , we find that the S/N becomes

$$\frac{S}{N} = 35 \sqrt{\frac{256 \times 256}{N_x N_y}} \left(\frac{N_g}{600} \right) \left(\frac{\sigma_0}{1} \right)^2 \quad (44)$$

This law was checked on a large number of numerical simulations.

For large N_g , the linear dependence of S/N with N_g is a strong gain of the ACF method compared to the standard method of coadding images method (BM) for which the signal-to-noise increases as $\sqrt{N_g}$. A comparison of the S/N for both the ACF and BM method is shown on Figure 2. In the case of deep observations (large N_g), the ACF will provide an easier and more accurate shear estimate from the shape matrix of the ACF than the coadded images of galaxies.

3.2.2. Effects of noise on the shear estimate

Because the gravitational shear is determined from the anisotropy of the ACF, the sources of noise on the ACF previously discussed affect the estimation of the shear. In particular, in the case of a single object, as for the ACF, the noise degrades



Fig. 2. Value of the signal-to-noise ratio for the ACF method (straight lines) and for the method of coaddition of images (lines proportional to the square-root), as a function of the total number of galaxies on the field N_g . The signal-to-noise of individual galaxies σ_0 corresponding to the different line styles are indicated.

the isophotes and randomly polarize the object. Consequently, in order to detect a significant non-zero shear value, the S/N ratio of the ACF must be sufficiently large, or, in other words, for a given value of S/N , only shear values greater than some threshold γ_0 can be detected with sufficient statistical significance.

Figure 3 is a result of a series of Monte-Carlo experiments where for each of them we measured the mean and the dispersion of the shear of 100 ACFs. Each ACF has a gaussian shape of 7 pixels diameter. Its true ellipticity γ_{true} is known, and the orientation is zero (i.e., we choose γ_{true} to be real). A noise pattern with a given dispersion and mean zero is added on each ACF; this fixes the S/N of the ACF. In each experiment, the 100 ACFs differ only in their noise pattern. We have performed 80 experiments, with 10 values of S/N , and 8 values of γ_{true} . The ellipticities are measured using the spatial filter (37) with a diameter $s = 6$ pixels. We also define the dispersion:

$$\sigma_\gamma = \sqrt{\langle [(\gamma_{\text{obs}1} - \gamma_{\text{true}})^2 + (\gamma_{\text{obs}2})^2] \rangle} \quad (45)$$

with $\gamma_{\text{obs}} = \gamma_{\text{obs}1} + i\gamma_{\text{obs}2} = |\gamma_{\text{obs}}| e^{2i\varphi}$. At a given value of the S/N , the threshold γ_0 is defined as a 1-sigma detection of the ellipticity:

$$\gamma_0 = \sigma_\gamma . \quad (46)$$

Figure 3a shows the relation between γ_{obs} , the observed ellipticity value of the ACF and γ_{true} , its true value. The apparent discrepancy is an effect of the spatial filter, and will be corrected with the calibration of the shear (see section 4.1). The quantitative dependence of γ_0 on the S/N of the ACF is plotted in Figure 3b.

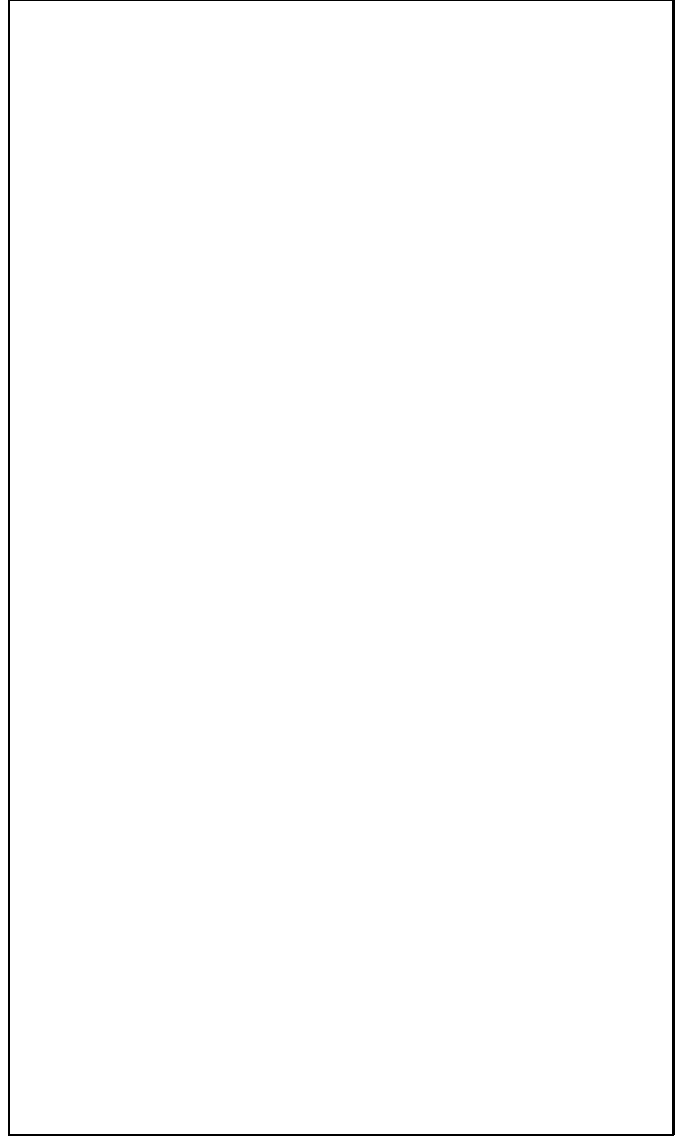


Fig. 3. The upper plot is the relation between γ_{obs} and γ_{true} . The proportionality constant is about a factor 4, and it is caused by the spatial filter (37) present in the second moment matrix (26). The lower plot is the 1-sigma detection level of the shear as a function of the S/N of the ACF.

3.3. Other sources of errors

3.3.1. Errors from the observational characteristics of the galaxies

The ACF method is ideal if the galaxies have the same flux, the same size, and the same profile. Unfortunately, this is not the case. A distribution in size, magnitude, and profile overweight some galaxies, and can change the *statistical properties* of the ACF. In principle, this could change the value of the shear. The detailed analysis of these effects, and how they could lead to new constraints on the faint galaxies properties, is a scope of the forthcoming PaperII. Nevertheless we can already propose a solution to the flux-weighting effect.

If the galaxies are distributed in flux, they would (if they had equal profile and equal size) contribute to the ACF in

proportion to the square of their flux; hence, the brightest galaxies could dominate the resulting ACF. However, this could be partly avoided in the following way: define $\gamma(\boldsymbol{\theta}_0; m > m_j)$ as the complex shear as determined from the ACF, which in turn has been determined by cutting out all objects on the frame brighter than m_j , as described in Sect.3.1.1. Selecting a set of flux thresholds m_j , and a set of weighting factors ν_j , $1 \leq j \leq M$, one can form the average

$$\langle \gamma(\boldsymbol{\theta}_0) \rangle = \frac{\sum_{j=1}^M \nu_j \gamma(\boldsymbol{\theta}_0; m > m_j)}{\sum_{j=1}^M \nu_j}, \quad (47)$$

which is an unbiased estimate of the shear at $\boldsymbol{\theta}_0$ for all choices of ν_j . Note that by an appropriate choice of the weight factors, the contribution by relatively bright galaxies can be suppressed. One can now try to choose the weight factors in such a way as to minimize the dispersion of the resulting estimate; this will be the topic of a future work.

A size and a profile distribution are expected to destroy the perfectly concentric shapes of the isophotes in the ACF. However, with the typical smoothing length we used (a Gaussian function with 0.8-1.5 arcmin radius), the galaxy number is sufficiently high on a 3-hours exposure at CFHT to make this effect negligible and to induce an almost noise-free and regular isophote pattern on the ACF.

3.3.2. Errors from the sources polarization distribution

The intrinsic ellipticities of galaxies induce statistical fluctuations on their mean ellipticity, i.e., on the shear estimated from that mean. If σ_ϵ is the dispersion of the intrinsic ellipticity distribution [assumed, as always, that this is isotropic, so that the mean of the (complex) ellipticity vanishes], then this intrinsic ellipticity distribution leads to a dispersion σ_{stat} of the resulting shear estimate of

$$\sigma_{\text{stat}} = \frac{\sigma_\epsilon}{\sqrt{N_g}}. \quad (48)$$

Thus, if the shear is determined from the ellipticity of individual galaxy images, this provides a limit on the possible accuracy of this measurement. The dispersion of the intrinsic ellipticity is easily determined from the data, since it nearly equals the dispersion of the observed galaxy images.

An intrinsic ellipticity distribution will also introduce a dispersion on the shear as estimated from the ACF; however, in this case the corresponding dispersion can be less securely estimated from the data itself. However, since the ACF method takes into account information from much fainter galaxies than can be detected and measured individually, we can take σ_{stat} as an upper bound on the dispersion introduced by the intrinsic ellipticity distribution.

3.3.3. Error from instrumental effects

The PSF is never circular, and an anisotropic correction of the shear estimate must be applied. The principal sources of anisotropies are known (see BM). It is possible to measure the anisotropy from stellar profiles and to model it by an instrumental deformation matrix A_{inst} as the gravitational deformation matrix introduced in Section 2.1, Eq.(2). A_{inst} does not contain the PSF, but only the instrumental deformation. By applying the inverse instrumental deformation matrix on the

shape matrix of the ACF, this deformation can be approximately corrected, as in Eq.(9) of Section 2.1:

$$\mathcal{M}_{\text{true}} = A_{\text{inst}}^{-1} \mathcal{M}_{\text{obs}} A_{\text{inst}}^{-1 t}. \quad (49)$$

As mentioned by BM, this approximation works provided that the instrumental deformation is constant in direction, and does not exceed 5-10 %.

3.4. Choice of the local smoothing length

The ACF is computed in a given smoothing window of the image where the distortion is supposed to be approximately constant. The characteristic size of this area is called the local smoothing length. Its typical scale must be optimized according to the limiting shear value and the typical spatial resolution we want to achieve. First, the number of galaxies N_g must be large enough for the statistical fluctuations of the resulting shear not to exceed the desired accuracy of the shear measurement. That is, σ_{stat} of Eq.(48) must be negligible when compared to $|\gamma_{\text{obs}}|$. Second, $|\gamma_{\text{obs}}|$ must be larger than γ_0 (see Fig.3b), which means that the S/N of the ACF must be sufficiently high. Since it is related by Eq. (44) to the number of galaxies, N_g is also constrained. The choice of the smoothing length is a compromise between these considerations. If it is too large, the small scales of the shear are averaged out. If it is too small, the noise and the statistical fluctuations induce a false value for the shear. Table 1 summarizes some constraints on N_g in the light of Sections 3.2.1 and 3.2.2. These values are only indicative since an exact model for the faint galaxies (size, profile, magnitude) is needed to make realistic predictions (see paper II). Such a realistic model will modify the law (44) and changes N_g .

Table 1. Lower limits on N_g required to measure a shear γ_0 in a superpixel of size 256×256 with faint galaxies.

γ_0	0.15	0.08	0.05	0.01
$N_n(\sigma_0 = 3.5)$	11	21	27	139
$N_n(\sigma_0 = 2.5)$	22	41	54	274
$N_n(\sigma_0 = 2.0)$	34	64	86	429
$N_n(\sigma_0 = 1.5)$	61	114	152	762
$N_n(\sigma_0 = 1.0)$	137	257	342	1714
N_{stat}	4	14	36	900

$N_n(\sigma_0)$ is the minimum number of galaxies with an individual S/N of σ_0 required in an area of 256×256 pixels (square-shaped top-hat window) to have a S/N of the ACF sufficiently large to measure a shear γ_0 . N_{stat} is the minimum number of galaxies required such that γ_0 is three times larger than σ_{stat} , assuming an intrinsic ellipticity dispersion of $\sigma_\epsilon = 0.1$ [see Eq.(48)].

Moreover, the choice of the smoothing length could depend on the position on the image since the shear varies spatially. Practically, an iterative procedure for the choice of this length is hampered by the very large computational time needed. An easier way is to find the mean “best” smoothing length from different tests. However, it should also be pointed out that for the reconstruction of the surface mass density of a cluster from

image distortions (e.g., Kaiser & Squires 1993; Fort & Mellier 1994; Seitz & Schneider 1995, and references therein) a spatially homogeneous dispersion on the observed shear appears to be optimal, i.e., as long as the shear estimate is unbiased, these reconstructions do not require that a shear different from zero is measured in each smoothing window.

4. Applications to data

Though the ACF method seems theoretically attractive, its efficiency has to be demonstrated on real CCD observations. In this section, we first show that the ACF method works on realistic simulated CCD images where a shear pattern has been introduced. In a second step, we analyse the shear field on real data corresponding to the two fields already studied by Bonnet et al. (1993, 1994).

4.1. Simulated images

We have used simulated images similar to those shown in BM and where photon noises, CCD defects, optical and atmospheric artifacts, or flat field residuals can be introduced. The ACF method is tested both on an image containing a lens, and on an image with no lens. Thus we can check that the method does not introduce spurious shear, and that the simulations provide an accurate calibration of the shear as well. Figure 4 shows the shear pattern as it is directly measured on the simulated image containing a lens. The smoothing length is a top-hat filter of size $50''$ which corresponds to about 30 galaxies detectable in each smoothing window. The ellipticity distribution is a flat distribution between 0.6 and 0.8. The resulting shear profile, azimuthally averaged with respect to the lens center, is displayed on Figure 5a. The errors bars are dominated by the statistical fluctuations of the galaxy ellipticities; they are determined from Eq.(48) using $N_g \simeq 30$. At the bottom, the 3 measured points before the calibration (49) are plotted (see subsection 3.2.2). To first order (weak shear approximation), the calibration is a multiplicative constant and does not depend on the value of the shear and the lens model. However, it does depend strongly on the PSF and the spatial filter used to compute the second moments of the ACF. The calibration is found from simulated sheared images which reproduce real image conditions on telescopes. The constant is the ratio of the observed (uncorrected) shear to the true shear. In Figure 5b, the shear profile after calibration of the unlensed image is shown. One sees that it is compatible with zero shear.

4.2. Real data

4.2.1. The shear around Q2345

The observation of a weak gravitational shear in the field of the double quasars Q2345+007A,B was made by Bonnet et al. (1993) from deep CCD images obtained at CFHT. This observational evidence of the gravitational origin of this doubly imaged quasar was confirmed later by Mellier et al. (1994), Fisher et al. (1994) and Pelló et al. (1996) who found an excess of galaxies centered on the shear pattern, and also close to the quasars. They revealed a fairly complex lens, probably composed of a distant cluster of galaxies and some bright nearby galaxies.

We analyse here the B and I images of Q2345 used in Bonnet et al. (1993), and we refer to this paper for the observa-

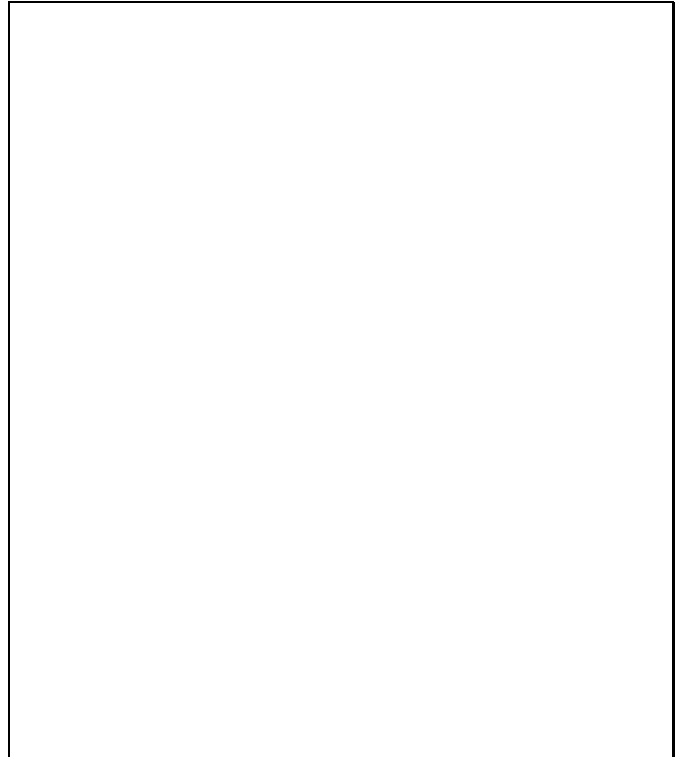


Fig. 4. Simulation of a 4 hours exposure at CFHT in the B band on a 3.5×3.5 field. The seeing is $0.7''$ with no tracking errors. Galaxies are lensed by an isothermal sphere ($\sigma = 1000\text{km/s}$), with a core radius of $4''$ located at $200''$ left from the field center. The lens redshift is 0.17 and the mean redshift of the sources is 1. The segments show the local orientation of the shear. Their length is proportional to the shear intensity.

tional details on the fields. We discard the I-band image for the shear analysis because the ACF is dominated by a crux pattern (see Figure 1) whose origin is unclear, but probably associated with residuals from the addition of many shift and add images which has been moved only along the pixel directions of the CCDs. Some residuals could be due also to bad charge efficiency. These defects are damaging for the shear analysis but they also reveal the high sensitivity of the ACF method (this suggests that the ACF could be also useful for testing CCDs).

Figure 6a shows the shear pattern found from a set of magnitude selected objects which clearly confirms the pattern found by Bonnet et al. (1993). 89 objects are detected in the blue magnitude range [26,27]. They are surrounded by a circle of size 30 pixels, whereas the rest of the image is put to zero. Since the galaxies are detected here using magnitude criteria, we adopt a completely different strategy than outlined before. The ACF is computed only from these selected objects since we detect galaxies here. The consequence is a considerable increase of the S/N of the ACF, compared to the case that the rest of the image was not put to zero. This is an interesting alternative of the coadding image in BM, since in the present approach, the centroid of the individual objects need not to be determined. However, the ultra faint objects are lost with this strategy. The objects are spatially ordered into 8 groups of 10 – 15 members, and the ACF is computed in each of these groups. Since the signal is highly significant

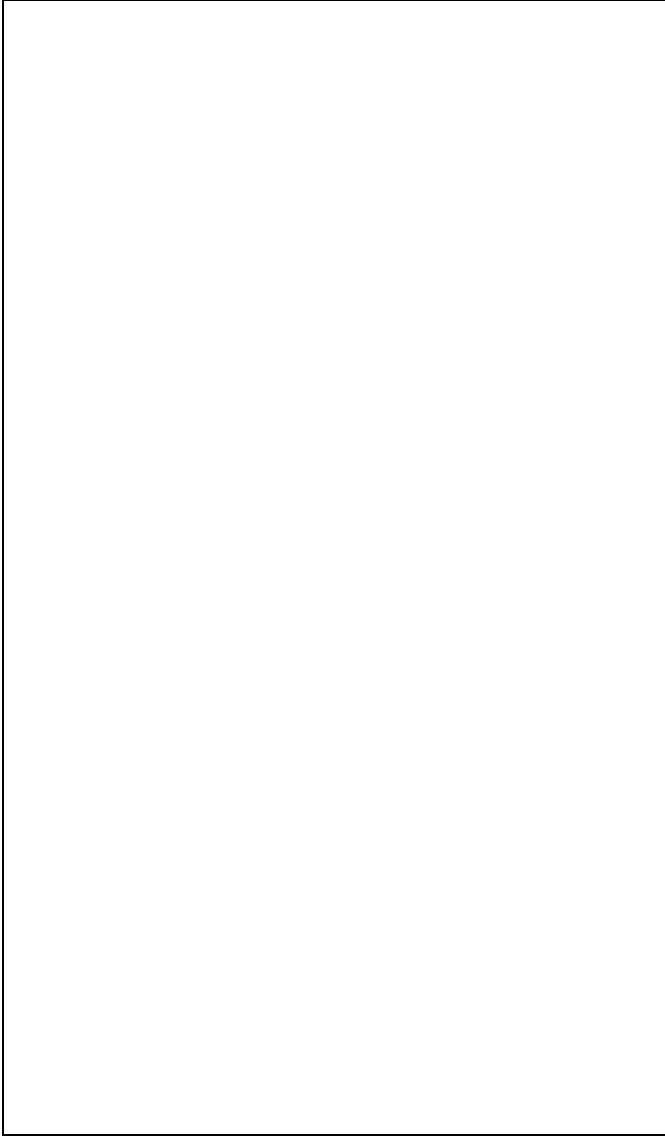


Fig. 5. (a) 1-dimensional shear profile from the simulation of Fig. 4. At the bottom the uncalibrated measure points are drawn. The theoretically expected shear profile is plotted as the dashed line. (b) The calibrated shear as measured from the simulation without a lens. The measured values are compatible with zero shear

($S/N \sim 40$), and the shear found is high (between 10 and 15 %), the measurement error is dominated by the intrinsic ellipticities of the galaxies. The probability that each segment (independently of the others) comes from a random orientation of the galaxies (the ellipticity dispersion is $\sigma_e = 0.2$) is around 10%. As in the Bonnet et al. paper, the shear is not corrected for tracking errors and PSF convolution since there are not enough stars to evaluate these effects (initially these observations were not done for measuring weak lensing!).

Figure 6b shows the shear pattern computed from the objects fainter than $m_B = 26.5$. The brighter galaxies are masked, as described in Sect.3.1.1, and the ACF is computed in a gaussian window of radius 0.9 . Since there are many more objects compared to Fig.6a, the S/N of the ACF is also high (~ 40), and the shear around the expected excess of galaxies responsi-

ble for the image splitting of the QSO is recovered. At least 30 objects are detectable in each smoothing window, which gives a lower limit of the confidence level per segment of 99%, assuming the same ellipticity distribution for the ultra-faint galaxy population as for the ones with $m_B = [26, 27]$. Remarkably, another shear pattern is detected with the same confidence level at the bottom of the image. Its superimposition with the I-band CCD image (Figure 6c) clearly reveals that the second shear pattern is centered on a visible excess of galaxies at the top-right of the I image. At first glance, the shape of this condensation is roughly elliptical and shows two density peaks. From the number of galaxies we see, it is probably a rather rich cluster of galaxies which has been undetected previously.

4.2.2. The shear around Cl0024

The central region of the cluster Cl0024+16 and an external region located at $6'$ from the cluster center were analysed by BMF, also from deep images obtained at CFHT. Again, we refer to this paper for details about the observations.

The shear analysis done with the ACF of the central part of Cl0024 is displayed in Figure 7a. The Gaussian smoothing length is $40''$, and the galaxies used are fainter than $m_B = 26.5$. The shape does not show differences with the BMF analysis but the coherence of the signal around the cluster center is stronger. The inner pattern clearly shows an elliptical shape oriented along the second bisecting line, indicating an elongated shape for the cluster along this direction. Furthermore, the innermost central region shows a significant signal in the direction perpendicular to the second bisecting line. This signal was not reported by BMF, probably because of the lower signal to noise ratio as compared with the ACF. Along with the general orientation reported above, the central shear resembles what is it expected for a bimodal mass distribution.

The shear analysis of the large external region is more interesting. The ACF method was used with 3 different magnitudes cuts, $m_V > 24$, $m_V > 25$, and $m_V > 26$. The corresponding shear maps are plotted in Figures 7b–d. For each segment, the smoothing length was $100''$. The general pattern found by BMF is also recovered here. The brightest map ($m_V > 24$) is really similar, and the probable perturbation also seems to be detected, at the same position, though with a lower significance level. The intermediate magnitude map looks similar to the former one, but the perturbation is no more visible. On the other hand, a significant signal appears at the top right corner (the northern side of the cluster). It could be an effect of a second clump. This signal increases significantly on the faintest map, and there is no doubt at all that it is real. Once we go further away from the cluster center, the signal become noisier than on previous maps, but on the other hand, close to the cluster center the intensity of the shear is even higher than on the brightest and intermediate magnitude shear map. It suggests that we may be less polluted by cluster galaxies at such faint magnitudes.

5. Conclusion

This paper presents a new approach to probe weakly distorted galaxies down to the background noise limit. Using the autocorrelation of the image enables us to increase the signal-to-noise ratio of the shear considerably, mainly for two reasons: (1) There is no more need to detect individual objects and to define individual centroids and individual shape parameters

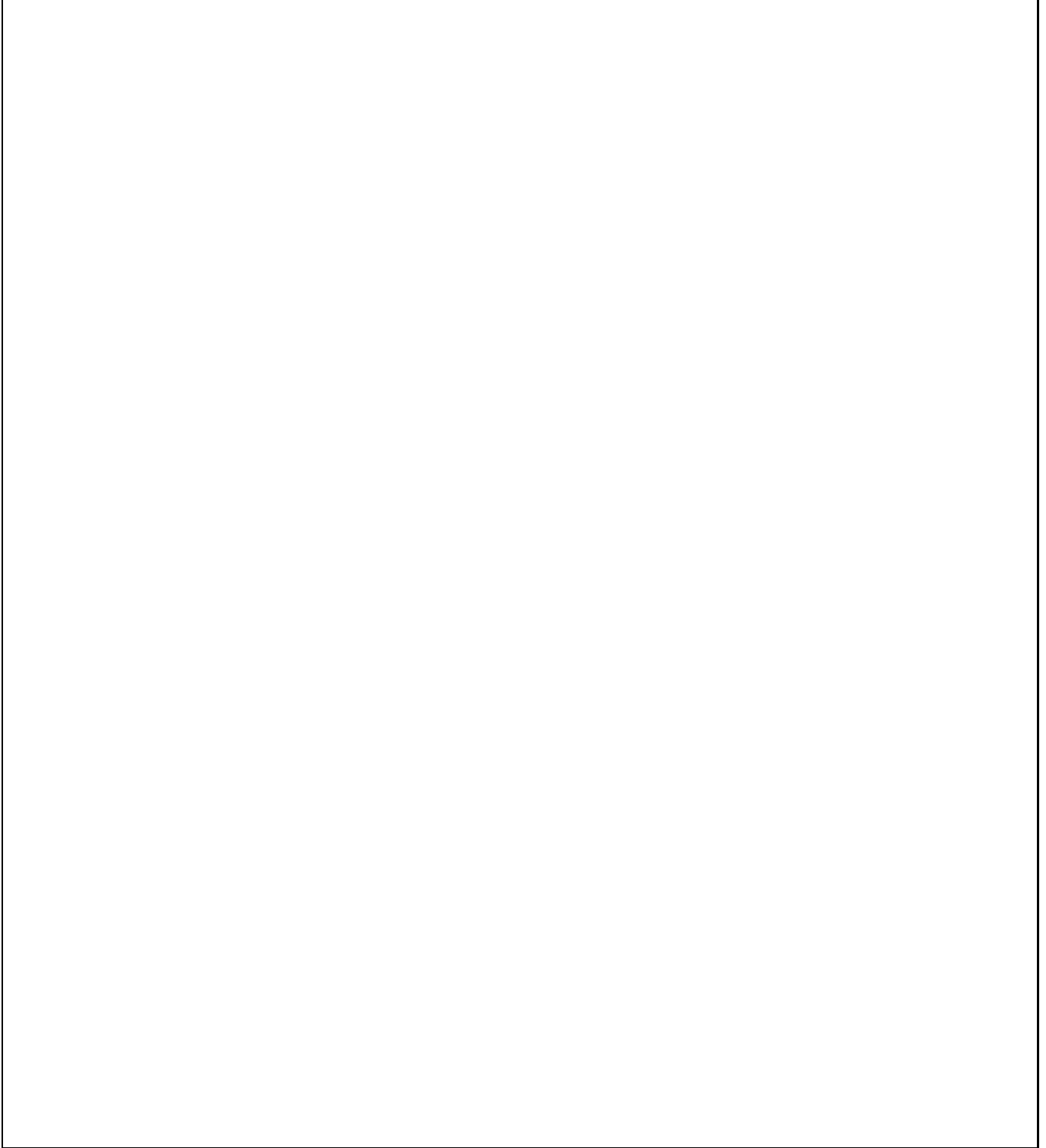


Fig. 6. Shear patterns found with the ACF method in the field of Q2345+007. (a) Shear pattern from 89 galaxies with $m_B=[26,27]$. (b) Shear pattern from the galaxies with $m_B > 26.5$. (c) The shear pattern from panel (b) overlaid onto the I-band image

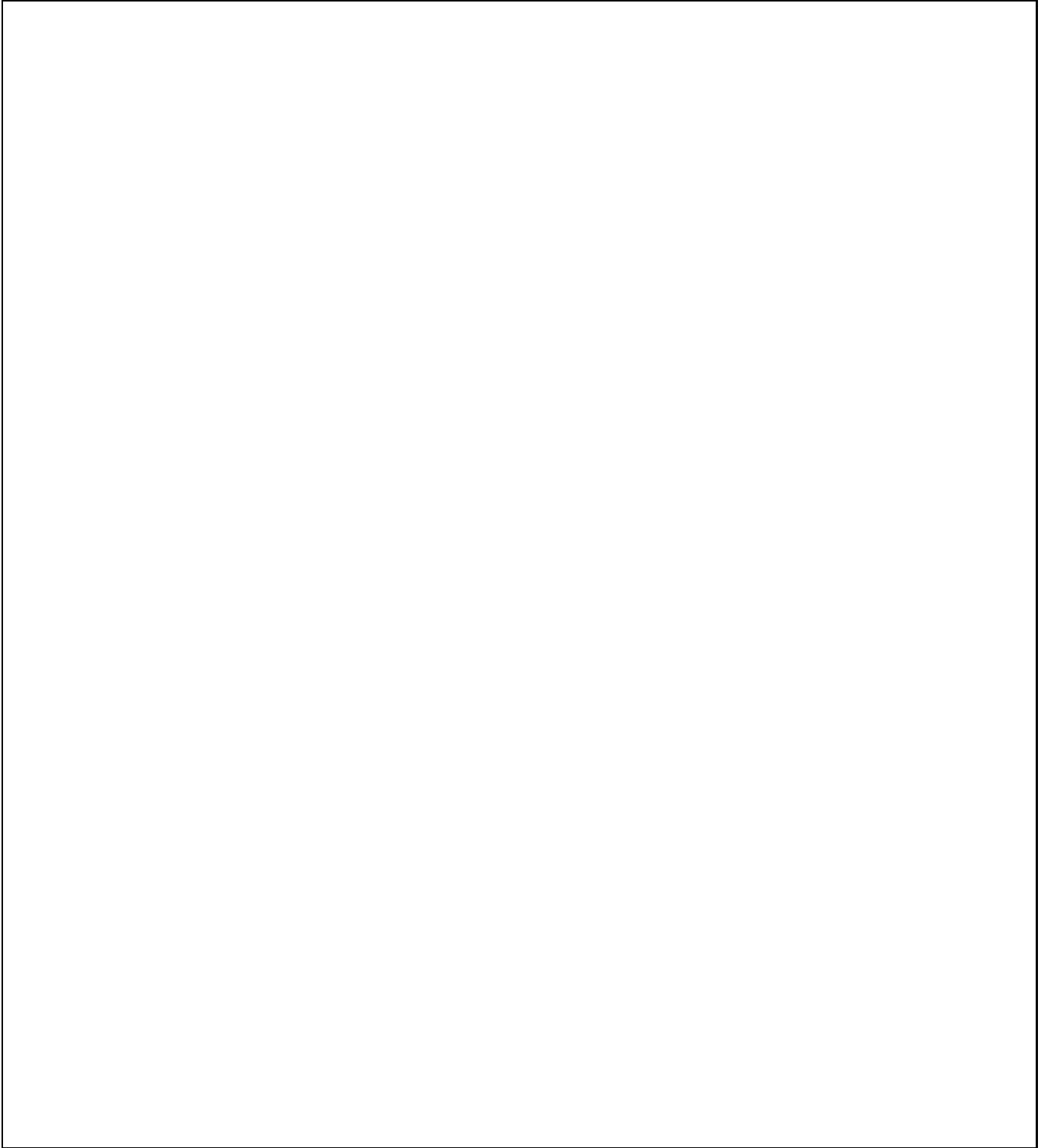


Fig. 7. Shear maps of Cl0024+1654 obtained with the ACF. (a) The central region of Cl0024+1654 with objects fainter than $m_B = 26.5$. The segments give the orientation and the intensity of the shear. The coherence is remarkable. Note also the inner shear pattern which seems oriented along the second bisecting line. The two large vertical segments at the bottom center of the image are artifacts generated after the merging of two CCD images which overlapped at this position. (b) External part Cl0024 with objects fainter than $m_V = 24$. The overall shape is similar as in BMF. Note the faint signal close to the perturbation reported by BMF which confirms that we probably detected a clump of matter toward this direction. (c) Same as (b) for galaxies with $m_V > 25$. The main difference to the previous one is the detection of a clear signal at the top right. (d) Same as (b) for galaxies with $m_V > 26$. The shear field at the top right is also significant and shows that another clump of matter must be located outside the field of view northward from the cluster center.

for these galaxies. (2) Even the faintest galaxies which cannot be detected by standard algorithms provide information to the ACF. Assuming there is a very dense population of distant background sources, they improve considerably the signal-to-noise ratio. A direct consequence of this correlation method is its ability to give upper bounds on these ultra-weak galaxies' number counts (see Paper II).

We have demonstrated that the ACF can be analysed as a single object whose geometry is related to the ACF of background sources modified by the gravitational shear. The second moments of the ACF computed over the whole field provides the magnification map, provided the ACF of the sources is known. Since the intrinsic ACF is due to very many faint galaxies, one can hope that it is a universal function, i.e., the same in each direction on the sky, so that it can be obtained from very deep HST images. The relation between the observed shear and the true shear inferred from the ACF can be determined (e.g., by simulations), and the instrumental/atmospheric degradations can be corrected in a standard way, provided the PSF is known, but with a strong benefit of the high signal-to-noise ratio of the ACF with respect to individual galaxies. In our approach we have implicitly assumed that this population is at high redshift, and does not correspond to low-redshift galaxies with low surface brightness.

The applications on simulated and real data are very encouraging. The ACF method easily recovers the shear profile found by BMF with another and independent method. However, as shown in the I-band image of Q2345+007, the drawback is the need of a very high quality of image acquisition. In particular, the shift and add method must be as random as possible, preferentially with no shift in columns and rows, to avoid privileged directions.

It is also possible to use the ACF method using only selected galaxies. The practical method is to select the objects with a given selection criteria (magnitude, or colour) and shade everything which is outside of a circle centered on each object. The ACF restricted to these objects can then be computed and analysed as was demonstrated here. This method was mentioned earlier by Kaiser (1992), though he did not go into further developments about its practical implementation.

We are aware that the ACF method is sensible to a flux, size, and profile distribution of the galaxies. Although we proposed a solution for the flux problem, the size and profile problem are more difficult and will be addressed later.

About the future developments, two main points must be kept in mind. First, the deep HST empty fields will help in the determination of the intrinsic correlation function. This leads to the simultaneous determination of both the magnification and the shear using the χ^2 minimisation (Eq. 33). However the question whether these empty fields are really empty is still open, though given that a one-dimensional function should be determined from observations (i.e., the radial profile of the isotropic intrinsic ACF), this does seem relatively easily possible. Second, the advantage of the ACF to avoid the reduction of data process (galaxy detection, first and second moment estimation) may be increased if a reliable deconvolution of the PSF on the ACF is possible. However, the proper difficulties of the deconvolution algorithms, in particular the uncertainties in the choice of the number of steps for the deconvolution process is still a source of problems.

The linear dependence of the S/N on the number of galaxies is a strong argument in favour of the ACF method for the

analysis of large fields where probably a small shear, but coherent over large angular scales, exists (e.g., Blandford et al. 1991, Kaiser 1992, Villumsen 1996, and references therein). The large number of ultra-faint galaxies is well adapted to the measurement of small shear.

Another question which should be investigated in future work is how the shear determined from the ACF method is combined with shear measurements with the 'standard method', i.e., from obtaining the average ellipticity of observed galaxy images. The combination should be made in such a way as to minimize the dispersion of the resulting shear estimate.

Acknowledgements We thank H. Bonnet, P.-Y. Longaretti, C. Seitz and S. Seitz for stimulating discussions, S. Roques and P. Marechal for enlightening discussions about the correlation function and M. Dantel-Fort, J. Bézecourt and J.-M. Miralles for their helps during the data reduction. This work was partly supported by the "Sonderforschungsbereich 375-95 für Astro-Teilchenphysik" der Deutschen Forschungsgemeinschaft (PS), l'Institut National de Sciences de l'Univers (INSU) and the Groupe de Recherche Cosmologie.

6. References

- Bartelmann, M., Narayan, R., 1995, ApJ, 451, 60.
 Blandford, R. D., Saust, A., Brainerd, T., Villumsen, J., 1991, MNRAS, 251, 600.
 Bonnet, H., Fort, B., Kneib, J.-P., Mellier, Y., Soucaill, G., 1993, A&A, 280, L7.
 Bonnet, H., Mellier, Y., Fort, B., 1994, ApJ 427, L83 (BMF).
 Bonnet, H., Mellier, Y., 1995, A&A, 303, 331 (BM).
 Brainerd, T., Blandford, R. D., Smail I., 1996, ApJ, in press.
 Broadhurst, T., Taylor, N., Peacock, J. A., 1995, ApJ, 438, 49.
 Dalcanton, J. J., 1996, SISSA preprint.
 Cole, S., Treyer, M.-A., Silk, J., 1992, ApJ 385, 9.
 Fahlmann, G. G., Kaiser, N., Squires, G., Woods, D., 1994, ApJ 437, 56.
 Fischer, P., Tyson, J. A., Bernstein, G., Guhathakurta, P., 1994, ApJ, 431, L71.
 Fort, B., Mellier, Y., 1994, A&AR, 5, 239.
 Kaiser, N., 1992, ApJ, 388, 272.
 Kaiser, N., Squires, G., 1993, ApJ, 404, 441.
 Kaiser, N., Squires, G., Broadhurst, T., 1995, ApJ, 449, 460.
 Mellier, Y., Dantel-Fort, M., Fort, B., Bonnet, H., 1994, A&A, 286, 701.
 Miralda-Escudé, J., 1991, ApJ, 380, 1.
 Pelló, R., Miralles, J.-M., Le Borgne, J.-F., Picat, J.-P., Soucaill, Bruzual, G., 1996, submitted.
 Schneider, P., Rix, H. W., 1996, ApJ, submitted.
 Schneider, P., Seitz, C., 1995, A&A, 294, 411.
 Schneider, P., Ehlers, J., Falco, E. E., 1992, *Gravitational Lenses*, Springer.
 Seitz, C., Schneider, P., 1995, A&A, 297, 287.
 Seitz, C., Kneib, J.-P., Schneider, P., Seitz, S. 1996, A&A, submitted.
 Smail, I., Hogg, D., Yan, L., Cohen, J. G., 1995, ApJ, 449, L105.
 Squires, G., Kaiser, N., Babul, A., Fahlmann, G. G., Woods, D., Neumann, D. M., Bohringer, H., 1996, in press.
 Van Waerbeke, L., Schneider, P., Mellier, Y., Fort, B., in preparation (Paper II).
 Villumsen, J., 1996, MNRAS, in press.